

Two-band parallel conductivity at terahertz frequencies in the superconducting state of MgB₂

M. Ortolani,¹ P. Dore,² D. Di Castro,² A. Perucchi,^{2,3} S. Lupi,^{2,3} V. Ferrando,⁴ M. Putti,⁴ I. Pallecchi,⁴ C. Ferdeghini,⁴ and X. X. Xi⁵

¹CNR-Istituto di Fotonica e Nanotecnologie, Via Cineto Romano 42, I-00156 Rome, Italy

²CNR-INFM Coherencia and Dipartimento di Fisica, Università di Roma La Sapienza, Piazzale Aldo Moro 2, I-00185 Rome, Italy

³Sincrotrone Trieste, Area Science Park, I-34012 Trieste, Italy

⁴CNR-LAMIA and Università di Genova, Via Dodecaneso 33, I-16146 Genoa, Italy

⁵Department of Physics, Pennsylvania State University, University Park, Pennsylvania 16802, USA

(Received 21 January 2008; published 24 March 2008)

The optical response of the two-band superconductor MgB₂ has been studied in the 0.7–4 THz range on films with very low impurity level. The effect of the high-energy σ gap is observed in the ratio R_S/R_N between the normal and superconducting state reflectance, while in a neutron irradiated film with a slightly higher impurity level, mainly the effect of the π gap is evident, as reported in previous experiments. At terahertz frequencies, the electrodynamics of MgB₂ can be well described by the two-band parallel conductivity model and is dominated by the π bands when the impurity level is only slightly higher than that of an ultraclean sample.

DOI: 10.1103/PhysRevB.77.100507

PACS number(s): 74.70.Ad, 74.25.Gz, 78.30.-j

The two-band superconductivity of MgB₂ has raised a lot of interest, and comprehensive theoretical and experimental studies of this material have been performed in the past years.¹ Thanks to the high T_c , the simple layered structure, the phononic origin of the superconducting pairing, and the amount of experimental and theoretical works already done, MgB₂ gives a unique opportunity for testing theoretical models of BCS superconductivity in the two-band case. Furthermore, MgB₂ epitaxial films are being extensively investigated for possible applications in superconducting devices and terahertz electronics.^{2,3} Infrared (IR) spectroscopy has largely contributed to the description of the physical properties of MgB₂, as discussed in detail in the recent comprehensive review of Kuzmenko.⁴ In the normal state, this technique can, indeed, distinguish the different contributions of the two bands (σ and π) to the frequency-dependent conductivity.⁴⁻⁷ In particular, reflectance measurements on the ab plane can provide values of the two corresponding plasma frequencies Ω_i and scattering rates $\gamma_i=1/\tau_i$ ($i=\sigma, \pi$). In the superconducting state, several studies have been performed in the terahertz or far-IR range (here defined by photon energies below 16 meV, frequency $\omega < 130$ cm⁻¹, or $\nu < 4$ THz) since a mark of the superconducting gap Δ is expected in the reflectance or transmittance spectrum at $\hbar\omega \sim 2\Delta$ (optical gap) for an isotropic s -wave BCS superconductor.

The most recent optical conductivity data from single crystals in the normal state show an overall consistency with band structure calculations.^{4,8} In the superconducting state, on the contrary, a two-gap description of the far-IR spectrum of MgB₂, based on independent BCS responses of σ and π bands, did fail in describing experimental data. In fact, the far-IR response of the ab plane of MgB₂ appears to be dominated by the π -band carriers.^{3,9-11} Indeed, no evidence of the high-energy gap Δ_σ was observed and a feature was generally seen at $\hbar\omega \sim 2\Delta_\pi$ in the ratio R_S/R_N (T_S/T_N), where R_S (T_S) and R_N (T_N) are the frequency-dependent reflectances (transmittances) in the superconducting and normal states, respectively. The BCS theory can be extended to the MgB₂

case by assuming a parallel sum of the conductivity of two independent bands with no cross terms, with each conductivity being described by a BCS model generalized to arbitrary temperature and γ_i values^{7,12} (for convenience, this model will be indicated hereafter as *generalized BCS model*). However, in the far-IR response evaluated with this model, the main feature shows up at $\hbar\omega \sim 2\Delta_\sigma$ when realistic values of the parameters Ω_i , γ_i , and Δ_i are employed.⁴ This inconsistency raises an important problem: while the dc transport properties and the dc-field penetration depth¹³ can be described under the two-band parallel conductivity assumption, the present body of experimental evidence suggests that this assumption can be questioned when applied at terahertz frequencies in the superconducting state.

The aim of the present work was to perform accurate measurements of the R_S/R_N spectrum in the far-IR range in order to verify the validity of the two-band parallel conductivity assumption. Since the small size of high-quality MgB₂ single crystals makes low-temperature measurements in the far-IR range very challenging,^{7,10} we used high-quality epitaxial films prepared by using a hybrid physical chemical vapor deposition, with $T_c=41$ K and optimal transport properties.¹⁴ The size of the film surface (5×5 mm²), with an average roughness of a few nanometers, allows for reflectance experiments in the whole infrared range, and the large film thickness ($d=200$ nm) strongly reduces the optical effect of the film substrate (see below). Since it is well known that MgB₂ samples quickly degrade in air in a few minutes,¹⁵ each film was sealed under vacuum in a quartz ampoule after growth and all the optical experiments were continuously performed in a vacuum of 10^{-6} mbar.

We performed Fourier transform-IR reflectance measurements at the infrared beamline SISSI at the synchrotron Elettra (Trieste, Italy) by using a He-flow cryostat, with a sapphire optical window and a cold finger, which allows positioning the prealigned sample and reference gold mirror on the incident beam with micrometric precision. We thus obtained the absolute reflectivity $R(\omega)$ from 2000 to 15 000 cm⁻¹ at 300 and 42 K. In the far IR, by exploiting the

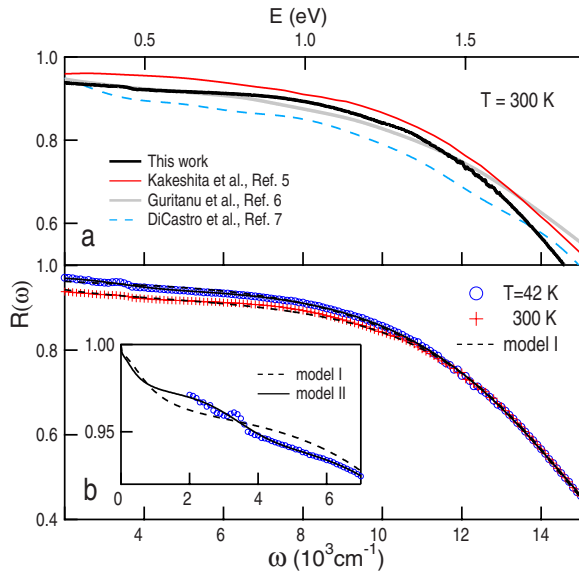


FIG. 1. (Color online) (a) Infrared reflectivity $R(\omega)$ of MgB_2 films from the present work as compared to that of crystals from Refs. 5, 6, and 10. (b) Drude–Lorentz fits to $R(\omega)$ (see text).

transparency of the sapphire window, we used synchrotron radiation to keep the focal spot size smaller than the film size with no loss of signal-to-noise ratio. We measured the intensity reflected by the sample by cycling the temperature in the 5–50 K range, without collecting the reference spectrum. In this way one avoids any variation in the sample position and orientation, which can produce frequency-dependent systematic errors in $R(\omega)$. By using the 42 K data as the normal state reference, we obtained $R(T)/R(42 \text{ K})$ spectra with an accuracy of $\pm 0.1\%$.

The agreement among room temperature $R(\omega)$ of the film and of single crystals^{5–7} is good [see Fig. 1(a)], indicating that the optical quality of our film is equivalent to that of single crystals. The $R(\omega)$ of the film measured at 42 K is compared with the one at 300 K in Fig. 1(b). As expected, $R(\omega)$ increases with decreasing temperature owing to the decrease of the scattering rates. We first performed a fit of $R(\omega)$ at 300 K by employing the Drude–Lorentz model including two Drude terms associated with the σ and π bands and a Lorentz contribution centered around $20\,000 \text{ cm}^{-1}$, representing an optically active $\sigma \rightarrow \pi$ interband transition (model I).^{5,6} We obtained an acceptable description of $R(\omega)$, as shown in Fig. 1(b), with $\Omega_\sigma = 3.8 \text{ eV}$, $\gamma_\sigma = 50 \text{ meV}$, $\Omega_\pi = 5 \text{ eV}$, and $\gamma_\pi = 370 \text{ meV}$ (the uncertainty on these values is of the order of 5%). These parameter values are consistent with previous ones,^{5,6} as expected on the basis of the consistency among the different reflectivity spectra (see Fig. 1). We note that the γ_i values at 300 K should be regarded as effective, model dependent values. Indeed, in a system like MgB_2 , characterized by a strong electron-phonon coupling, the simple Drude model is inadequate at mid-IR frequencies. The extended Drude model,⁶ in which both scattering rate and effective mass are frequency dependent, should be applied instead. However, the generalization of the latter model to the two-band case is well beyond the scope of this Rapid Communication.

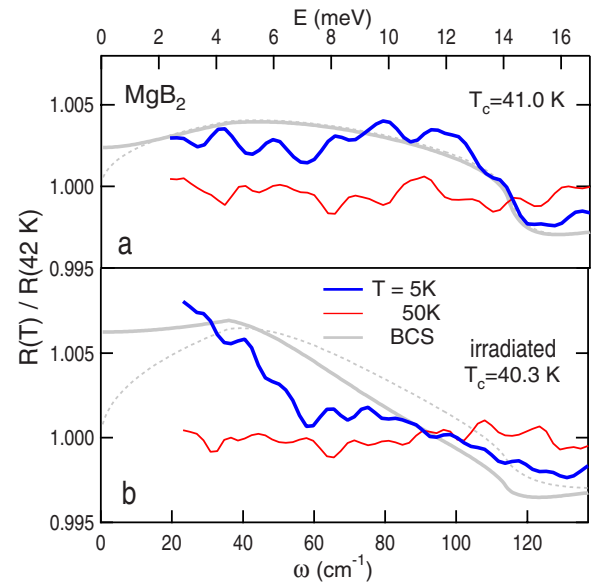


FIG. 2. (Color online) Far-infrared reflectivity ratio (thick blue line) as compared to BCS calculations (thick gray line, film thickness $d = 200 \text{ nm}$; dotted line, semi-infinite medium) with $\Omega_\sigma = 3.8 \text{ eV}$, $\gamma_\sigma = 11 \text{ meV}$ [$\gamma_\sigma = 37 \text{ meV}$ in (b)], $\Delta_\sigma = 7.2 \text{ meV}$, $\Omega_\pi = 5 \text{ eV}$, $\gamma_\pi = 75 \text{ meV}$, and $\Delta_\pi = 2.3 \text{ meV}$.

At 42 K, by using the same values of the plasma frequencies, the agreement between the measured spectrum and the best-fit curve is not satisfactory below 6000 cm^{-1} , as shown in the inset of Fig. 1(b). The agreement with data is significantly improved if a mid-IR Lorentz oscillator at 0.4 eV is included (model II). Although this oscillator may be partially due to the $\sigma \rightarrow \sigma$ interband excitation observed in a previous single-crystal measurement,⁷ it should be mainly regarded as an effective tool to compensate the above mentioned inadequacy of model I at mid-IR frequencies. Therefore, the 42 K best-fit scattering rates provided by model II ($\gamma_\sigma = 11 \text{ meV}$, $\gamma_\pi = 75 \text{ meV}$) do correctly describe the conductivity at far-IR frequencies, where the effect of the 0.4 eV oscillator is negligible. We remark that these γ_σ and γ_π values are only determined by intrinsic impurities owing to the vanishing phonon population at low temperatures in MgB_2 (Refs. 16 and 17) and are close to those previously reported for a single crystal [$\gamma_{\sigma, \text{imp}} = 12.4 \text{ meV}$, $\gamma_{\pi, \text{imp}} = 85.6 \text{ meV}$ (Ref. 6)].

As regards far-IR results, the $R(T)/R(42 \text{ K})$ measured at 50 and 5 K are shown in Fig. 2(a). For $T > T_c$, as expected, the $R(T)/R(42 \text{ K})$ curve is flat within experimental uncertainties, while on decreasing temperature below T_c , the $R(T)/R(42 \text{ K})$ spectrum increases and a clear edge structure around 14 meV becomes evident at $T = 5 \text{ K}$. We remark that the high accuracy of the present synchrotron measurements allows for the detection of an effect as small as $\sim 0.5\%$. To discuss this result, we calculated the R_S/R_N ratio by using the generalized BCS model introduced above and compared it to $R(5 \text{ K})/R(42 \text{ K})$. As input parameters, we employed the Ω_i and γ_i values at 42 K reported above and the Δ_i values obtained by tunneling spectroscopy on films of the same kind [$2\Delta_\sigma = 14.4 \text{ meV}$, $2\Delta_\pi = 4.6 \text{ meV}$ (Ref. 18)]. The R_S/R_N

spectra obtained by considering both a finite film thickness ($d=200$ nm) and a semi-infinite medium⁴ are not appreciably different, as shown in Fig. 2(a). By remarking that the model spectra are not the best fit to the data but are results of calculations with no free parameters, the resemblance with the data is highly significant. In particular, an edge structure at around 14 meV due to the σ gap is observed in both experimental and model spectra, while in previous works, it was concluded that the far-IR response is dominated by the π bands since an edge was observed between 4 and 7 meV in all cases (see Refs. 9 and 10, and Ref. 4 for a review). The observation of the 14 meV edge is a crucial result, since it finally allows us to reconcile the far-IR observation with the predictions of BCS calculations. We remark that this result has been obtained on a film with very low impurity level¹⁴ and minimal exposure to the atmosphere. We will thus refer to this sample as the *ultraclean* film.

To investigate the effect of the impurity level, we performed far-IR measurements on a second film, which was previously irradiated with thermal neutrons (fluence of 10^{16} particles/cm). The preparation and physical properties of irradiated films are fully described in Refs. 17, 19, and 20. A high fluence of 10^{19} particles/cm is known to suppress superconductivity in MgB₂ because of the production of a huge amount of lattice defects.²¹ On the contrary, in the case of a low-fluence irradiated film like the one we investigated, the density of lattice defects is too small to modify the band structure or the electron-phonon coupling and only an increase of the impurity scattering rates is observed, as shown by residual resistivity ρ_0 ,²⁰ Andreev reflection,²² and critical field and specific heat¹⁷ measurements. The measured reflectivity ratio $R(T)/R(42\text{ K})$ is shown in Fig. 2(b) for $T=50$ and 5 K. A clear edge is evident at around 7 meV, i.e., around $2\Delta_\pi$, while a much smoother increase close to the noise level is observed below 12 meV.

In a film from the same batch as the one we investigated and irradiated with the same fluence (sample IRR15 in Ref. 20), the $T_c=40.3$ K and the gap values measured by tunneling spectroscopy²³ are very close to those of unirradiated films, while ρ_0 increases by a factor ≈ 2 .²⁰ This effect can be mainly attributed to an increase of γ_σ , as shown by a detailed analysis of magnetoresistance data¹⁹ and by recent first-principle computations.²⁴ In a reasonable approximation, the R_S/R_N ratio can be evaluated within the generalized BCS model by using the same parameters of the ultraclean film case, with the exception of γ_σ increased from 11 to 37 meV. This value matches $\gamma_\pi/\gamma_\sigma=2.0$ evaluated for the IRR15 sample in Ref. 24 and it is also compatible with the above cited increase of ρ_0 . A reasonable agreement is obtained among the experimental data and the model spectra in Fig. 2(b) evaluated for both the $d=200$ nm film and a semi-infinite medium in the well accessible spectral range, i.e., above 4 meV. The difference between experimental and model spectra occurring at around 7 meV is unclear at the moment, and a more refined model should be employed to explain its origin. By remarking that the model curve results not from a best fitting procedure but from an independent calculation, the general agreement between model and data indicates that, when the scattering rates are slightly higher than those of the ultraclean film, the far-IR spectrum appears

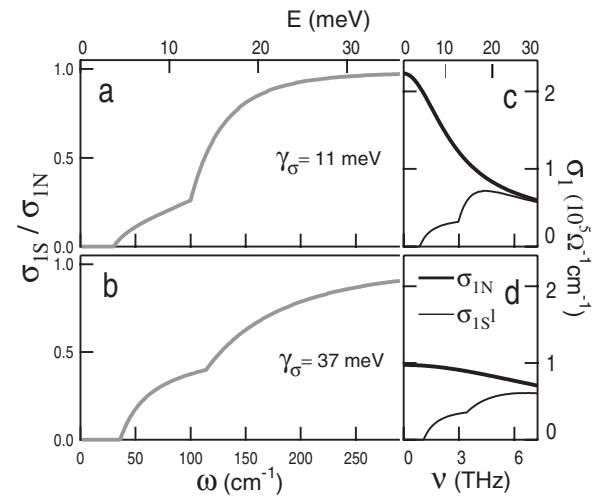


FIG. 3. [(a) and (b)] Optical conductivity change across the transition calculated from a BCS model (see text) with parameters as in Fig. 2. [(c) and (d)] Conductivity evaluated through the Drude model (normal state, thick lines) and BCS model (superconducting state, thin lines). 1 THz corresponds to 33 cm^{-1} or 4.1 meV .

to be dominated by the π -band carriers, as previously observed in a number of MgB₂ samples.^{7,9-11}

For a more straightforward interpretation of the far-IR data, we now discuss the obtained results in terms of the real part of the optical conductivity $\sigma_1(\omega)$. In particular, by using the two-band generalized BCS model, we evaluated σ_{1S}/σ_{1N} since the optical gaps, appearing as absorption edges in this ratio, can be clearly evidenced. For the ultraclean film, the σ_{1S}/σ_{1N} was obtained by using the parameters quoted above as input: $\Omega_\sigma=3.8$ eV, $\gamma_\sigma=11$ meV, $\Delta_\sigma=7.2$ meV and $\Omega_\pi=5$ eV, $\gamma_\pi=75$ meV, $\Delta_\pi=2.3$ meV. The model curve in Fig. 3(a) exhibits two gaps, one at $2\Delta_\pi=4.6$ meV and the other at $2\Delta_\sigma=14.4$ meV, with the latter being more evident. The curve in Fig. 3(b) was obtained by changing only the parameter γ_σ to 37 meV, which is the same value we choose to model the reflectivity of the irradiated film in Fig. 2. The curve in Fig. 3(b) displays a clear gap feature at $2\Delta_\pi$, while the gap at $2\Delta_\sigma$ is much less evident. The inspection of the separate σ_{1N} and σ_{1S} curves shown in Figs. 3(c) and 3(d) may elucidate the difference between the two cases. σ_{1N} of Fig. 3(c) is dominated by the narrow Drude contribution described by Ω_σ and γ_σ , which decreases abruptly with frequency. As a consequence, a sharp absorption edge in σ_{1S}/σ_{1N} is observed at around $2\Delta_\sigma$ in Fig. 3(a). In Fig. 3(d), σ_{1N} decreases more slowly with ω owing to a larger γ_σ , then in Fig. 3(b), a smoothed edge in σ_{1S}/σ_{1N} appears at around 5 meV. As discussed above, the second set of parameters models a MgB₂ sample with an impurity level slightly higher than that in the ultraclean case, the optical conductivity curves in Figs. 3(b) and 3(d) fail to display a clear two-edge structure, a situation previously reported for both MgB₂ films^{3,9,11,25} and single crystals.^{7,10} This analysis can explain why the effect of the high-energy gap due to the σ bands can be unambiguously observed only in samples with a very low impurity level and indicates that the two-band parallel conductivity model can describe fairly well the terahertz con-

ductivity of MgB_2 in both normal and superconducting states, even if the two-gap features are not clearly separated.

In conclusion, we performed IR reflectivity measurements on high-quality MgB_2 films. We find a close correspondence between our far-IR R_S/R_N spectrum and that predicted by a generalized BCS model assuming a parallel sum of the conductivity of two independent bands. Far-IR measurements on a film with a slightly higher impurity level lead to a R_S/R_N spectrum in which only the effect of the low-energy π gap is well evident, thus explaining the inconsistency between

theory and previous far-IR or terahertz experiments in terms of different impurity levels. Of general interest is the proof that the parallel sum of the conductivity of two superconducting bands can well describe the electrodynamic response of MgB_2 at terahertz frequencies.

The work at Penn State was supported in part by NSF under Grant No. DMR-0306746 and by ONR under Grant No. N00014-00-1-0294. M.O. acknowledges support from BESSY and IB-Berlin.

-
- ¹S. Tajima, I. Mazin, D. van der Marel, and H. Kumakura, *Physica C* **456**, 1 (2007).
- ²S. Cherednichenko, V. Drakinskiy, K. Ueda, and M. Naito, *Appl. Phys. Lett.* **90**, 023507 (2007); Ke Chen, Y. Cui, Qi Li, X. X. Xi, Shane A. Cybart, R. C. Dynes, X. Weng, E. C. Dickey, and J. M. Redwing, *ibid.* **88**, 222511 (2006).
- ³B. B. Jin, P. Kuzel, F. Kadlec, T. Dahm, J. M. Redwing, A. V. Pogrebnnyakov, X. X. Xi, and N. Klein, *Appl. Phys. Lett.* **87**, 092503 (2005).
- ⁴A. B. Kuzmenko, *Physica C* **456**, 63 (2007).
- ⁵T. Kakeshita, S. Lee, and S. Tajima, *Phys. Rev. Lett.* **97**, 037002 (2006).
- ⁶V. Guritanu, A. B. Kuzmenko, D. van der Marel, S. M. Kazakov, N. D. Zhigadlo, and J. Karpinski, *Phys. Rev. B* **73**, 104509 (2006).
- ⁷D. Di Castro, M. Ortolani, E. Cappelluti, U. Schade, N. D. Zhigadlo, and J. Karpinski, *Phys. Rev. B* **73**, 174509 (2006).
- ⁸G. Satta, G. Profeta, F. Bernardini, A. Continenza, and S. Massidda, *Phys. Rev. B* **64**, 104507 (2001).
- ⁹J. J. Tu, G. L. Carr, V. Perebeinos, C. C. Homes, M. Strongin, P. B. Allen, W. N. Kang, E. M. Choi, H. J. Kim, and S. I. Lee, *Phys. Rev. Lett.* **87**, 277001 (2001).
- ¹⁰A. Perucchi, L. Degiorgi, J. Jun, M. Angst, and J. Karpinski, *Phys. Rev. Lett.* **89**, 097001 (2002).
- ¹¹J. H. Jung, K. W. Kim, H. J. Lee, M. W. Kim, T. W. Noh, W. N. Kang, H. J. Kim, E. M. Choi, C. U. Jung, and S. I. Lee, *Phys. Rev. B* **65**, 052413 (2002).
- ¹²W. Zimmermann, E. H. Brandt, M. Bauer, E. Seider, and L. Genzel, *Physica C* **183**, 99 (1991).
- ¹³A. A. Golubov, A. Brinkman, O. V. Dolgov, J. Kortus, and O. Jepsen, *Phys. Rev. B* **66**, 054524 (2002).
- ¹⁴A. V. Pogrebnnyakov, J. M. Redwing, S. Raghavan, V. Vaithyanathan, D. G. Schlom, S. Y. Xu, Q. Li, D. A. Tenne, A. Soukassian, X. X. Xi, M. D. Johannes, D. Kasinathan, W. E. Pickett, J. S. Wu, and J. C. H. Spence, *Phys. Rev. Lett.* **93**, 147006 (2004).
- ¹⁵Y. Cui, J. E. Jones, A. Beckley, R. Donovan, D. Lishego, E. Maertz, A. V. Pogrebnnyakov, P. Orgiani, J. M. Redwing, and X. X. Xi, *IEEE Trans. Appl. Supercond.* **15**, 224 (2005).
- ¹⁶T. Masui, *Physica C* **456**, 102 (2007).
- ¹⁷M. Putti, M. Affronte, C. Ferdeghini, P. Manfrinetti, C. Tarantini, and E. Lehmann, *Phys. Rev. Lett.* **96**, 077003 (2006).
- ¹⁸M. Iavarone, R. Di Capua, A. E. Koshelev, W. K. Kwok, F. Chiarella, R. Vaglio, W. N. Kang, E. M. Choi, H. J. Kim, S. I. Lee, A. V. Pogrebnnyakov, J. M. Redwing, and X. X. Xi, *Phys. Rev. B* **71**, 214502 (2005).
- ¹⁹I. Pallecchi, V. Ferrando, E. Galleani D'Agliano, D. Marre, M. Monni, M. Putti, C. Tarantini, F. Gatti, H. U. Aebersold, E. Lehmann, X. X. Xi, E. G. Haanappel, and C. Ferdeghini, *Phys. Rev. B* **72**, 184512 (2005).
- ²⁰V. Ferrando, I. Pallecchi, C. Tarantini, D. Marre, M. Putti, C. Ferdeghini, F. Gatti, H. U. Aebersold, and E. Lehmann, *J. Appl. Phys.* **101**, 043903 (2007).
- ²¹R. H. T. Wilke, S. L. Bud'ko, P. C. Canfield, J. Farmer, and S. T. Hannahs, *Phys. Rev. B* **73**, 134512 (2006).
- ²²D. Daghero, A. Calzolari, G. A. Ummarino, M. Tortello, R. S. Gonnelli, V. A. Stepanov, C. Tarantini, P. Manfrinetti, and E. Lehmann, *Phys. Rev. B* **74**, 174519 (2006).
- ²³R. Di Capua, H. U. Aebersold, C. Ferdeghini, V. Ferrando, P. Orgiani, M. Putti, M. Salluzzo, R. Vaglio, and X. X. Xi, *Phys. Rev. B* **75**, 014515 (2007).
- ²⁴M. Monni, I. Pallecchi, C. Ferdeghini, V. Ferrando, A. Floris, E. Galleani d'Agliano, E. Lehmann, I. Sheikin, C. Tarantini, X. X. Xi, S. Massidda, and M. Putti, *Europhys. Lett.* **81**, 67006 (2008).
- ²⁵A. V. Pronin, A. Pimenov, A. Loidl, and S. I. Krasnosvobodtsev, *Phys. Rev. Lett.* **87**, 097003 (2001).